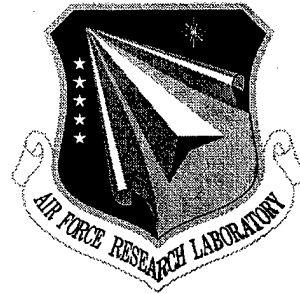AFRL-IF-RS-TR-1999-193
Final Technical Report
September 1999

WIDEBAND PHOTONICS ELECTRIC FIELD SENSOR

SRICO Inc.

S. Sriram

APPROVED FOR PUBLIC RELEASE; DISTRIBUTION UNLIMITED.

AIR FORCE RESEARCH LABORATORY
INFORMATION DIRECTORATE
ROME RESEARCH SITE
ROME, NEW YORK

19991015 031

This report has been reviewed by the Air Force Research Laboratory, Information Directorate, Public Affairs Office (IFOIPA) and is releasable to the National Technical Information Service (NTIS). At NTIS it will be releasable to the general public, including foreign nations.
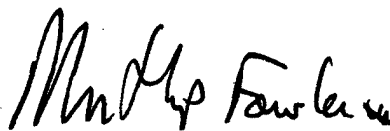
AFRL-IF-RS-TR-1999-193 has been reviewed and is approved for publication.

APPROVED:

Christopher Reuter
Project Engineer

FOR THE DIRECTOR:

Northrup Fowler, III, Technical Advisor
Information Technology Division
Information Directorate

REPORT DOCUMENTATION PAGE

Public reporting burden for this collection of information is estimated to average 1 hour per response, including the time for reviewing instructions, searching existing data sources, gathering and maintaining the data needed, and completing and reviewing the collection of information. Send comments regarding this burden estimate or any other aspect of this collection of information, including suggestions for reducing this burden, to Washington Headquarters Services, Directorate for Information Operations and Reports, 1215 Jefferson Davis Highway, Suite 1204, Arlington, VA 22202-4302, and to the Office of Management and Budget, Paperwork Reduction Project (0704-0188), Washington, DC 20503.

1. AGENCY USE ONLY (Leave blank)	2. REPORT DATE	3. REPORT TYPE AND DATES COVERED
	September 1999	January 1997-September 1998

4. TITLE AND SUBTITLE
WIDEBAND PHOTONICS ELECTRIC FIELD SENSOR

5. FUNDING NUMBERS
C - F30602-97-C-0038
PE - 62702F
PR - 2338
TA - 03
WU - PG

6. AUTHOR(S)
S. Sriram

7. PERFORMING ORGANIZATION NAME(S) AND ADDRESS(ES)
SRICO Inc.
2724 Sawbury Blvd
Columbus Ohio 43235

8. PERFORMING ORGANIZATION REPORT NUMBER

0001 AD

9. SPONSORING/MONITORING AGENCY NAME(S) AND ADDRESS(ES)
Air Force Research Laboratory/IFTC
Information Directorate
26 Electronic Pkwy
Rome New York 13441-4514

10. SPONSORING/MONITORING AGENCY REPORT NUMBER

AFDRL-IF-RS-TR-1999-193

11. SUPPLEMENTARY NOTES
AFRL Project Engineer: Christopher Reuter/IFTC/ (315) 330-3808

12a. DISTRIBUTION AVAILABILITY STATEMENT
Approved for Public Release; Distribution Unlimited

12b. DISTRIBUTION CODE

13. ABSTRACT (Maximum 200 words)

SRICO developed a wideband photonics electric field sensing system capable of measuring signals up to 18 GHz. The electric field sensor is a passive integrated optic Mach-Zehnder interferometer device. The sensor is made from all-dielctric materials without any electrical connections.

14. SUBJECT TERMS
Sensor   Electric Field   Integrated Optics   Optical Isolation

15. NUMBER OF PAGES
36

16. PRICE CODE

17. SECURITY CLASSIFICATION OF REPORT	18. SECURITY CLASSIFICATION OF THIS PAGE	19. SECURITY CLASSIFICATION OF ABSTRACT	20. LIMITATION OF ABSTRACT
UNCLASSIFIED	UNCLASSIFIED	UNCLASSIFIED	UL

Table of Contents

List of Figures

Introduction

Electromagnetic fields are suspected of causing system upset and failure on Air Force platforms (Ref. 1). An understanding of the electromagnetic environment at the time of system upset or failure would greatly improve the operation of the system from the standpoint of reliability, reparability and maintainability. To characterize the EM environment requires a wideband sensor that permits the discrimination of multiple frequencies.

To do this, the Air Force contracted SRICO to develop a photonic wideband electric field sensor. This novel all-optical electric field sensor uses fiber and integrated optics technologies. One unique advantage of this sensor is that it eliminates the use of metallic antenna or electrical connections which can interfere with the accurate measurement and characterization of the EM environment. Because SRICO's electric field sensor is an all-optical device and an all-dielectric device, it offers minimal disturbance to the electric field to be measured. (Ref. 2)

The function of the wideband photonic electric field sensor is to characterize the electromagnetic environment. The electric field to be measured, in which this electric field sensor is immersed, modulates an optical beam which is guided through the sensor. The exiting optical beam carries information about the field strength and frequency spectrum of the electric field. A schematic of the photonic electric field sensor system is shown below in Figure 1.
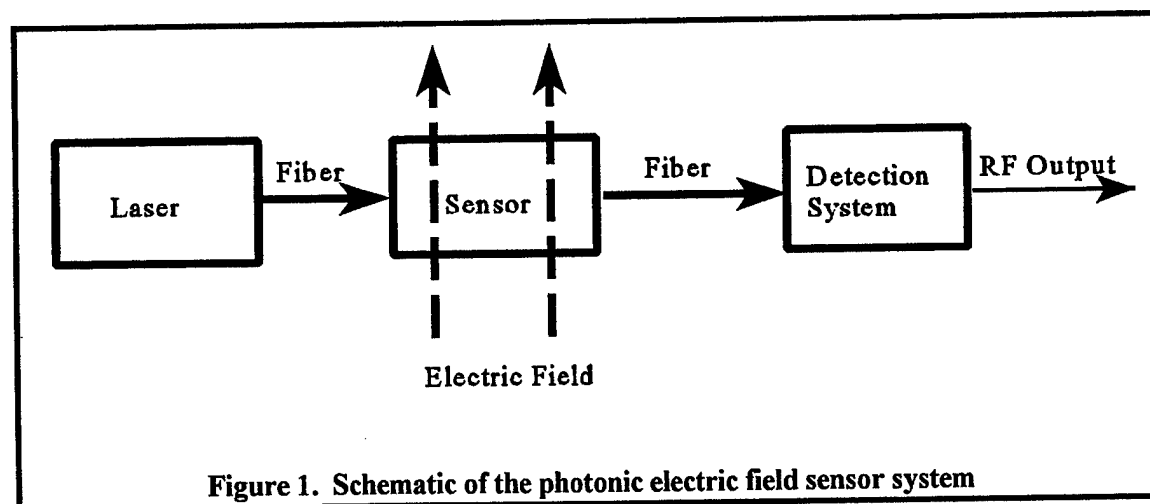
Figure 1. Schematic of the photonic electric field sensor system

The sensor system uses a laser whose output is provided as input to the photonic electric field sensor. The electric field sensor is placed in the EM environment. The optical output of the sensor is modulated by the electric field present in the EM environment. The optical output, which is a linear representation of the electric field present in the EM environment is provided to an optical fiber. The output optical fiber is connected to a detection system consisting of an optical receiver and low-noise preamplifiers. The RF output of the detection system is processed and recorded as needed.

Features
Several key features of the optical electric field sensor make it superior to electrical devices for electric field measurement.

- The sensor is an optical component
- The sensor output is an optically modulated signal
- The sensor is compatible with the optical fiber used for input and output
- The sensor has no electrical connections
- The sensor does not require any power supply at the sensing head

Benefits
SRICO's photonic electric field sensor has many benefits over the electrical devices.

- The sensor provides improved measurement accuracy by reducing susceptibility to electrical noise because the sensor is made of dielectric materials
- The sensor provides non-contact measurement of electric field
- The sensor may be placed in hostile or remote areas because optical fibers can send signal over long distances with high fidelity
- The sensor is electrically isolated providing operator and instrumentation safety
- The sensor is small enough to be used where space is a constraint

Electric Field Sensor

The fabricated electric field sensor component, shown in Figure 2, is a novel all-optical device that uses fiber and integrated optics technologies. One unique advantage of this sensor is that it eliminates the use of a metallic antenna or electrical connections which can interfere with accurate measurement and characterization of the electromagnetic environment. The sensor is packaged with optical fibers for input and output. The optical fibers enable remote measurement of the field from a safe distance of 100 meters.

The small size and ruggedness of the product is made possible by the successful formation of an integrated version of a Mach-Zehnder interferometer, a particular optical interferometer configuration (Ref. 3). The Mach-Zehnder interferometer is fabricated in an electro-optically active lithium niobate crystal substrate using the technologies of integrated optics. The electric field sensor uses the electro-optic properties of lithium niobate to phase modulate the light propagating in each arm of the Mach-Zehnder interferometer. This phase modulated optical signal is converted to intensity modulation at the output of the interferometer.
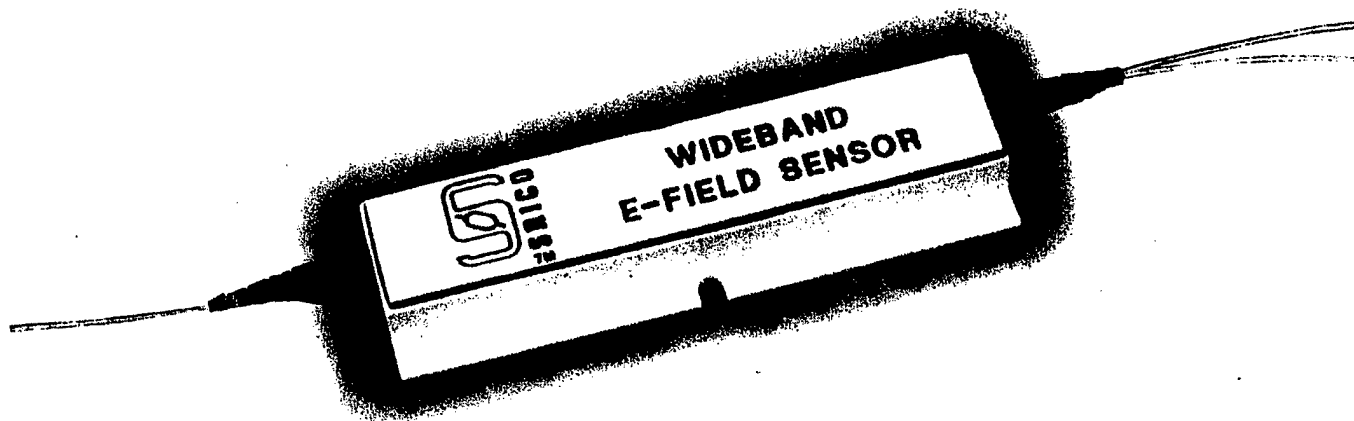

Figure 2. Photograph of the photonic electric field sensor fabricated

3

Device Theory

Schematic of the electric field sensor configuration is shown in Figure 3. The schematic shows reverse-poled regions in the two waveguide channels. The circle showing the reverse-poled region 1 in the top channel and an equal length in the bottom channel form an electrode-less E-field sensing section. The reverse-poled region 2 in the bottom channel is used to compensate for the temperature effects caused by the reverse-poled region 1. This section is shielded from the electric field by a metal layer. The optical waveguide circuit is a Mach-Zehnder interferometer designed for operation up to 18 GHz. This device structure has an input Y-branch and an output directional coupler. Light input to the sensor is received from a polarization maintaining single mode fiber. Light output from the sensor is connected to standard single mode fibers.

The applied electric field produces equal and opposite phase shifts in the optical beam propagating in the two channels, thereby leading to a net phase shift of twice the phase shift per channel. When the two optical beams recombine at the output directional coupler the phase modulation is converted to an amplitude modulated signal at the same frequency of the applied electric field. The optical signal amplitude is proportional to the applied electric field.

The directional coupler is designed to divide the output equally between the two channels. This is referred to as a 3 dB splitter. The two optical output are equal but opposite in phase for this condition. One major benefit of the 3 dB directional coupler is that the Mach-Zehnder interferometer is biased at quadrature, thus, eliminating the need for a bias voltage. This is a passive device.
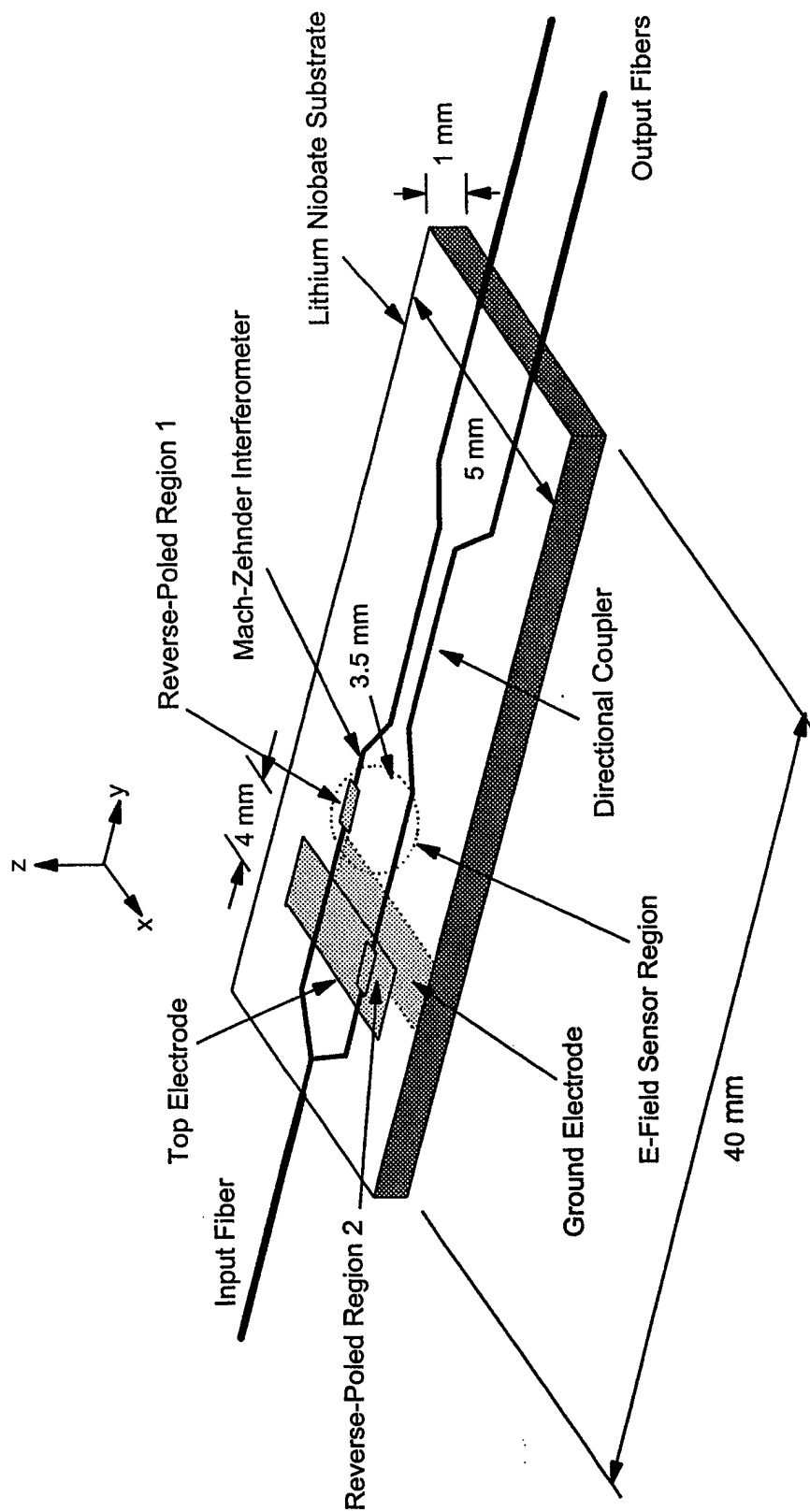
Figure 3. Schematic of the photonic electric field sensor

Theory

In the device structure shown in Figure 3, the Z-directed uniform electric field produces the electric field, E_z, inside the crystal. Since the electric field in the waveguides is only in the Z direction, E_x and $E_y = 0$. Only E_z is a non-zero component of the electric field vector.

This Z-directed electric field interacts with the optical beam propagating in the waveguide to produce electro-optic modulation. The electric field vector of the optical wave propagating in the waveguide is also oriented in the Z direction. This optical wave is referred to as the Transverse Electric (TE) mode. This electric field produced by the applied electric field modifies the refractive index of the crystal through the linear electro-optic effect. The refractive index along the Z axis (or the c axis), referred to as the extraordinary index, is n_e. The change in n_e is given by (Refs. 4, 5)

$$\Delta n_e = -\frac{1}{2} n_e^2 r_{33} E_z \tag{1}$$

where,

n_e is the extraordinary index of refraction of lithium niobate (2.15)

r_{33} is the electro-optic coefficient of lithium niobate (30×10^{-12} m/V)

Equation 1 describes the change in the refractive index in each leg of the interferometer due to electric field. The phase change in the optical beam propagating in each leg of the interferometer is

$$\Delta \phi_1 = -\frac{\pi}{\lambda} n_e^3 r_{33} E_z L \tag{2}$$

where,

λ is the wavelength of the light propagating in the waveguide (1300 nm)

L is the length of the reverse-poled region 1 in Fgirue 3 (3.5 mm)

The device configuration shown in Figure 3 operates in a push-pull fashion. Because of the arrangement of the reverse poled region, the second leg of the interferometer sees the opposite polarity of electric field. Thus, the phase change associated with the second leg of the interferometer is, therefore, opposite in sign to that of the first leg, i.e.,

$$\Delta \phi_2 = \frac{\pi}{\lambda} n_e^3 r_{33} E_z L \tag{3}$$

The total phase change is

$$|\Delta \phi_1 - \Delta \phi_2| = |\Delta \phi_t| \tag{4}$$

$$|\Delta \phi_t| = 2 \frac{\pi}{\lambda} n_e^3 r_{33} E_z L \tag{5}$$

6

The phase shift produced by the electric field in each channel is converted to amplitude or intensity modulation at the output of the interferometer. The optical signal output of the interferometer, at quadrature bias ($\phi = \pi/2$), is approximated by

$$P_s = \frac{P_i}{2} [1 - \Delta\phi_t \ (E)] \qquad (6)$$

where P_i is the input power (assuming a lossless interferometer).

The above equation shows that the output optical power is linearly proportional to the net phase shift which is a linear function of the electric field. Since this is a linear device, the detected optical signal is at the same frequency as the voltage signal. Thus, the optical signal, P_s, would yield the necessary information regarding the electric field being measured.

The complementary outputs of the directional coupler design of interferometer which was illustrated in Figure 3, yields significant improvements in the dynamic range of the sensor. This complementary or push-pull output characteristic is illustrated in Figure 4. With complementary photodetection, a basic 3 dB improvement in signal-to-noise ratio may be obtained. In the complementary (push-pull) topology of Figure 3, common-mode intensity noise can be reduced by as much as 30 dB. This allows lower-cost but rather noisy fabry-perot laser diodes to be employed, rather than the expensive, but quiet distributed feedback (DFB) laser diodes, or expensive and bulky solid state Nd:YAG lasers.
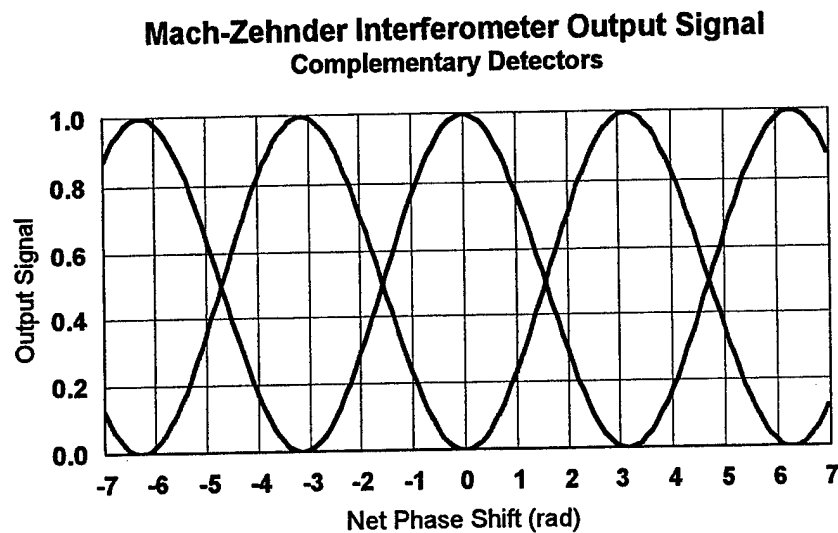
Mach-Zehnder Interferometer Output Signal
Complementary Detectors

Figure 4   Complementary cosine-squared interference transmission characteristics of a Mach-Zehnder interferometer with output directional coupler

Device Fabrication

This section briefly describes the technology used to fabricate the electric sensor with input and output optical fibers.

Electric Field Sensor

The device fabrication requires three photomasks. The first photomask defines the titanium diffusion to create the reverse poled region. The second photomask defines the proton exchange waveguides which form the Mach-Zehnder interferometer device. The third photomask defines the electrode structure on the reverse poled region of the second leg of the interferometer.

The crystal end faces are polished to obtain high quality surfaces for attaching input and output optical fibers. Individual sensor devices are cut or diced from the crystal substrate.

Fiber Attachment

The polarization maintaining optical fiber attached to the electric field sensor is manufactured by 3M Specialty Fiber. It is coated with a 400 micron diameter acrylate coating. The fiber is pulled through a 1 mm diameter teflon tube for protection and ease of handling.

The polarization maintaining fiber consists of a core and two stress rods along one of the fiber diameters. These stress rods are easily seen under 1000X magnification. This fiber has two well defined orthogonal polarization axes, known as the fast axis and the slow axis. The phase velocity of light polarized along the fast axis is slightly higher than that along the slow axis. The fast axis is identified as the direction which is normal to the line joining the center of the two stress members.

Each 1 meter fiber cable is fabricated as a pigtail. Each fiber pigtail is connectorized with a FC/APC type fiber optic connector. Angle Polished Connectors (APCs) are employed to substantially increase the return loss from optical reflections which would otherwise cause major amplitude fluctuations in the detected signal as the temperature changed or the fiber cable moved. The slow axis of the fiber is aligned with the keyway on the connector. The other end of the fibers are cleaved for attachment to the voltage sensing device. The optical input to this sensor device should be along the TE polarized direction and this is conveniently supplied through the use of a polarization maintaining (PM) optical fiber. The fiber is oriented such that the laser light is launched along its fast axis.

The optical fibers are attached to the polished crystal end-faces. The optical fibers are attached to the Mach-Zehnder interferometer sensor waveguide by placing them in a glass carrier which provides both precision fiber positioning capability and mechanical support to the fiber.

Special micromanipulator equipment is used to align the fast axis of the fiber in the fiber carrier with the waveguide in the $LiNbO_3$ crystal for fiber attachment. The light from the laser is polarized and launched along the fast axis of the fiber. The core of the input fiber is aligned with the channel waveguide at the input of the device. The output of the waveguide is collected with a microscope lens (20X) and detected with an optical power meter. The fiber is aligned using micromanipulator equipment with sub-micron precision. The alignment of the input fiber can be adjusted with respect to all six degrees of freedom to achieve optimal coupling. Optimal coupling is achieved when the detected throughput is a maximum. Once coupling is optimized, a drop of UV epoxy is applied in the gap between the fiber carrier and the sensor. The epoxy is then cured using a UV source.

9

The output fiber carrier, containing the two single-mode output fibers, is aligned with the output of the sensor after the input carrier has been epoxied and cured. The throughput is measured by coupling the output from the fibers into optical power meters. The output is optimized for both outputs simultaneously. The output fiber carrier is epoxied in the same manner as the input, described above.

The input and output fibers are connectorized with FC/APC connectors and the sensor device is placed in a plastic box.

System Considerations

The following theory shows how the dynamic range of the electric field sensing system can be measured. The signal-to-noise ratio of the output from the optical receiver is mainly dependent on the amount of optical power at the photodetectors and the intensity modulation depth produced by the electric field applied to the sensor. To determine this theoretical value, the carrier-to-noise ratio is first determined. A technique for increasing the dynamic range by about 20dBby suppressing the optical carrier is also shown.

Carrier-To-Noise Ratio

In a direct detection optical system the Carrier-To-Noise Ratio is given by (Ref. 6):

$$CNR = \frac{(\frac{\eta . e . P_c}{h f_c})^2 R_L}{[\frac{2 . \eta . e^2 P_c R_L}{h f_c} + 4 . k . T . F_s] . B_n} \qquad (7)$$

where η = quantum efficiency (0.6),
  e = electronic charge (1.6×10^{-19} C),
  P_c = mean optical power at the photodetector (2 mW),
  h = Planck's constant (6.63×10^{-34} J.s),
  f_c = frequency (2.31×10^{14} Hz),
  R_L = load resistance (50 Ω).
  k = Boltzmann's constant (1.38×10^{-23} J/K),
  T = temperature (300 K),
  F_s = effective Noise Figure of receiving system (6 dB),
  B_n = effective noise bandwidth (20 GHz).

The numerator corresponds to the signal power developed in the photodetector load resistance. The denominator corresponds to the noise. The first term in the denominator is the quantum noise produced by the statistical arrival of the photons. For the above parameters at a wavelength of 1.3 microns, this noise power component has a value of -64.0 dBm in the 20 GHz bandwidth. It is assumed that the laser source has virtually no excess intensity noise. This is reasonably true for solid-state sources like the Lightwave Electronics Model 125 laser diode pumped Nd:YAG laser, which has a high frequency shot noise floor within 2 dB of the theoretical quantum noise.

The second term in the denominator is that associated with the thermal noise of the receiving system. It has a value of -58.8 dBm. Because the thermal noise is 5.2 dB higher than the quantum noise, this receiver is said to be "kT noise limited". The receiver is said to be "quantum noise limited" if the quantum noise is equal or greater than the kT noise. The ideal situation for maximum sensitivity and dynamic range is when the quantum noise is at least 10 dB greater than kT noise. It is not possible to achieve even the quantum-noise limited threshold condition with high bandwidth optical receivers due to photodetector saturation limitations, as this would require received optical powers greater than +8 dBm (6.3 mW).

11

For the values associated with Equ. (1), the signal power in a receiver system presenting an effective load of 50 Ω is 78 μW or -11.1 dBm. Based on the above calculated values of quantum and kT noise, -64.0 dBm and -58.8 dBm, respectively, the total noise floor is-57.6 dBm. Thus, the CNR, which is the difference between the signal power and the noise floor, is 46.5 dB.

For a substantially quantum noise-limited detection, Equ. (1) reduces to the well-known expression:

$$CNR = \frac{\eta P_c}{2.h f_c.B_n} \qquad (8)$$

The corresponding CNR for this situation is 52.9 dB. Thus, because 2 mW of optical carrier power is insufficient for quantum noise limited detection in this receiver, the CNR is degraded by 6.4 dB.

Signal-To-Noise Ratio

Having established the CNR, it now needs to be seen how the Signal-To-Noise Ratio (SNR) relates to CNR. If a sinusoidal modulating tone is applied to the sensor, its optical output intensity is modulated according to the following relationship:

$$P_m = [1 + m.\sin(2.\pi f_m.t)]P_c \qquad (9)$$

where P_m = modulated carrier power or intensity,
         m = modulation index ($\ll 1$),
         f_m = modulation frequency,
         t = time.

For the analog intensity modulation of a high frequency signal, $m \ll 1$ for linearity considerations. For such a device the peak phase modulation in the interferometer is $\Delta\phi$ ($\ll 1$).

The Signal-To-Noise Ratio (SNR) is related to the CNR by:

$$SNR = \frac{m^2}{2}.CNR \qquad (10)$$

If we assume that m or $\Delta\phi$ = 0.1, then SNR = CNR - 23 dB. Earlier we calculated that CNR = 46.5 dB. Thus, the corresponding SNR = 23.5 dB. We can thus see why it is so difficult to obtain high dynamic ranges in wideband fiber optic systems. One thing we would normally do to increase the CNR for a given received optical power would be to insure that the receiver was quantum noise limited. This we would do with a transimpedance amplifier to increase the effective photodetector load and hence lower the threshold for the quantum noise limit. Unfortunately, this option is not available at frequencies above about 1 GHz, due to the unavailability of suitable microwave transimpedance amplifiers. Even if such transimpedance amplifiers were available, the increase in CNR and SNR would only be 6.4 dB. We are left with only one option, and that is to increase the received optical power. However, photodetector saturation with present-day devices prevents us from attempting this, even when ample laser power is available.

12

Optical Carrier Suppression

One solution to this problem, as indicated earlier, is to suppress the optical carrier by attenuating the power in the carrier component that provides no useful information (Refs. 7, 8). This concept is illustrated in Figure 5, in both the frequency and time domains, for the response to an optical carrier with one set of sidebands, offset by $\pm f_m$. If FSR = $2f_m$, and the optical filter tuned to place a notch at the carrier frequency f_c, then the intensity of the carrier component can be reduced by about 20 dB, without substantially affecting the sidebands. The tuning of the filter can be achieved by electrically heating the filter substrate. The commercial optical filter product offered by Photonic Integration Research, Inc. (PIRI) has a temperature tuning coefficient of 0.01 nm/°C (2.7 GHz/°C). Alternatively, the optical carrier frequency can be tuned. The latter is easily done with a Lightwave Electronics Nd:YAG laser, which can be tuned over about 18 GHz before longitudinal mode hopping and over hundreds of GHz across many modes. Thus, there is no problem in centering the filter precisely on the optical carrier component. It can be maintained at the correct operating frequency using closed-loop control of the substrate heater or cooler or of the laser frequency.

Since the modulation sidebands are 26 dB down on the carrier component for $m = \Delta\phi = 0.1$, we could attenuate the carrier by 20 dB and still be able to linearly detect the modulation. What we would do, in fact, would be to attenuate the carrier by 20 dB and increase the laser power by the same amount. So that, if 2 mW of optical power normally reached the photodetector, the laser power could be increased to 200 mW and after modulation it could be attenuated by 20 dB. This would cause the power detected to be still only 2 mW - the saturation power of the photodetector. It has been assumed for convenience that before the filtering process, most of the energy is contained in the carrier component. After the carrier has been partially suppressed and the power increased, the mean power in the signal remains essentially the same. Now the power in the sidebands would be increased by 20 dB, causing a 20 dB increase in the detected signal power and SNR.
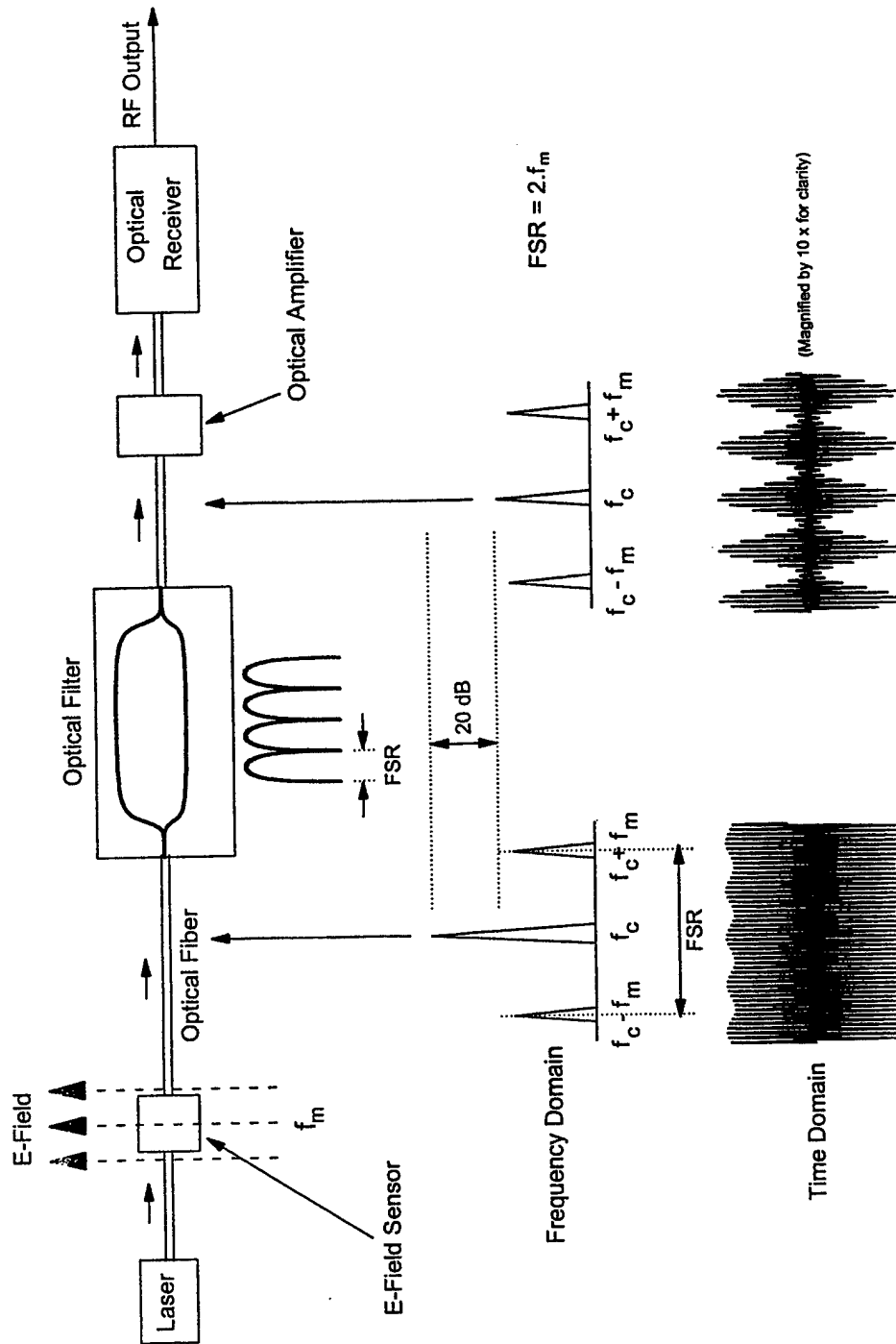
13

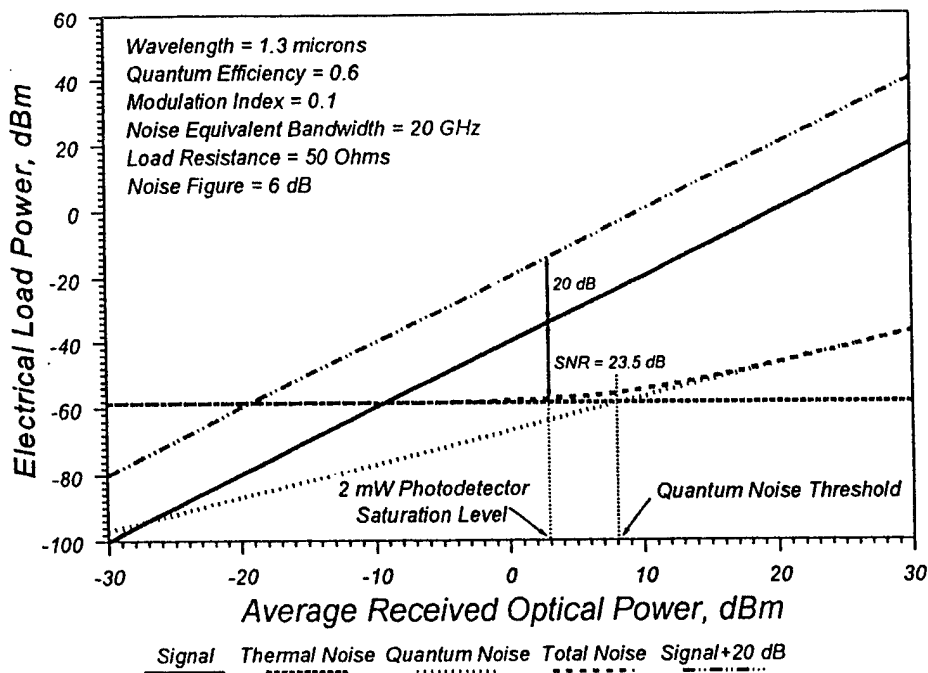**Figure 5. Carrier suppression technique to increase the dynamic range**

**Figure 6. Graph showing signal and noise levels as
a function of received optical power**

Figure 6 summarizes the foregoing and illustrates graphically how the dynamic range can be improved by about 20 dB - nearly doubling (in dBs) the available dynamic range, from 23.5 dB to 43.5 dB. As previously noted, a typical photodetector saturation level for cw signals is about +3 dBm (2 mW), whereas, the quantum (shot) noise threshold is at +8 dBm (6.4 mW). As baseband bandwidths increase above 20 GHz, the advantage of the extra 20 dB of dynamic range becomes even more apparent. Indeed, without this extra dynamic range, such optical systems would not be viable for links that required very large instantaneous bandwidths.

Normally, the optical carrier filter would be placed just before the photodetector, as is illustrated in Figure 5. However, in some long links using very coherent laser sources (such as the Lightwave Electronics laser used in the CATV industry), there would be an advantage in placing the filter immediately after the intensity modulator, before the light is launched into the fiber. For this would help mitigate non-linear effects that degrade system performance that can occur in long single-mode optical fibers, i.e., Brillouin and Raman Scattering.

Post Detection Optimization

The post-detection subsystem was optimized to reduce the effective system Noise Figure to a low value. The Noise Figure of the post detection stage following the optical receiver was reduced to about 2.5 dB when used with the HP8593E Spectrum Analyzer.

15

Test Results

The electric field sensor was tested over a wide frequency range. The low frequency test was conducted by placing the sensor inside a TEM cell and the high frequency test was conducted by placing the sensor inside a metallic waveguide. Test results are presented that show increase in dynamic range by using an optical filter.

Low Frequency Test, 10MHz to 1 GHz

Figure 7 shows a schematic diagram of the laboratory system for testing the electric field sensor over the frequency range of 10MHz to 1GHz. The fiber pigtailed electric field sensor is placed within a Crawford TEM Cell, IFI Model CC110. The optical fibers are fed through the sloping walls of the TEM cell and connected to the laser and the photodetector via FC/APC fiber optic connectors.

The optical source is a low-noise Nd:YAG laser, Model 125 manufactured by Lightwave Electronics, Inc., operating at 1.3 micron wavelength. The optical receiver, Model 1611, is manufactured by New Focus, Inc. The output of the optical receiver is amplified by about 20dB using a low-noise amplifier.
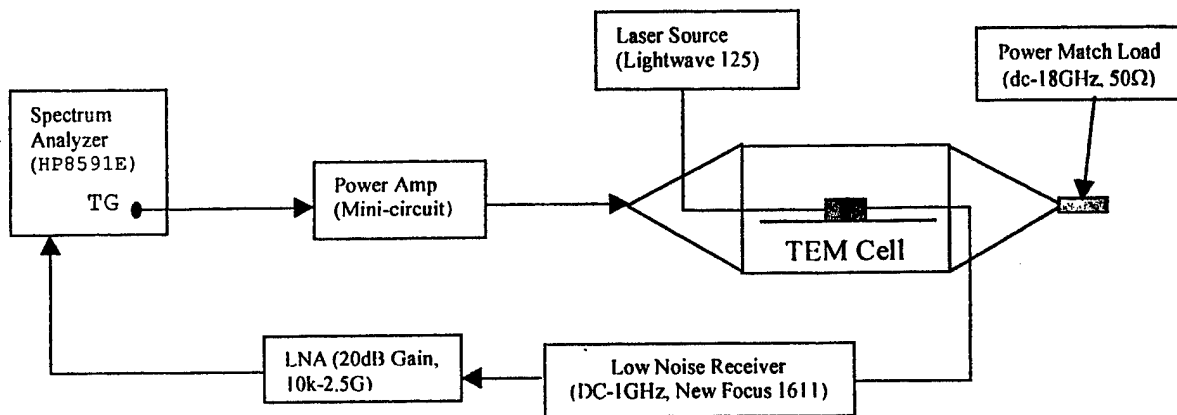

Figure 7. Low frequency test set up

16

The RF input to the TEM cell is supplied by the Tracking-Generator available in the HP8591E Spectrum Analyzer. The ouput of the Tracking-Genearator is amplified to a level of +30dBm (1Watt) which is then applied to the TEM cell. The dimensions of the TEM cell are such that 1 Watt of RF power produces a peak electric field of 168 Volts /meter. The RF power travels through the TEM cell in the same direction as the propagation of light in the optical fibers and the electric field sensor.

Figures 8 and 9 show the system noise floor and the measured signal by sweeping the Tracking-Generator over the frequency range of 10MHz to 1.1 GHz. The noise floor and signal measured at 509MHz are -129 dBm/Hz and -57.5 dBm, respectively. Therefore, the internal electric field of 168 Volts/meter produces an SNR of 72 dB. The minimum detectable electric field is

$$E_{min} = 168 \times 10^{-\frac{72}{20}} = 42 \ (mV/m/\sqrt{Hz}) \tag{11}$$

The exact electric field would be determined after calibrating the sensor to a known field strength.
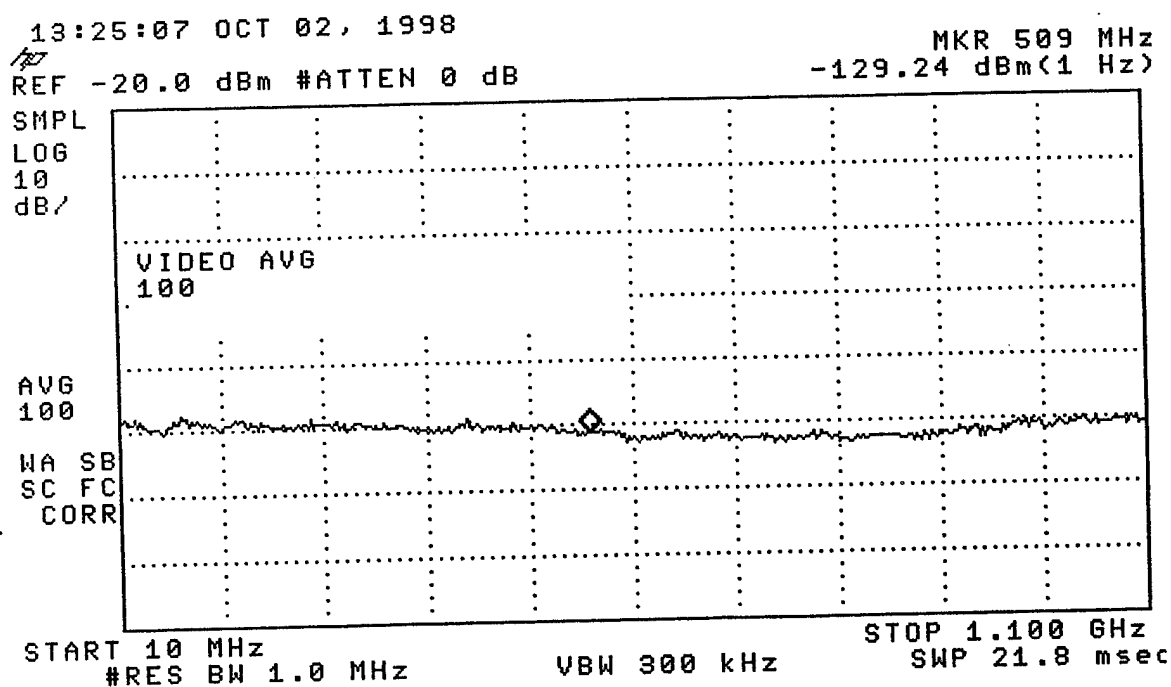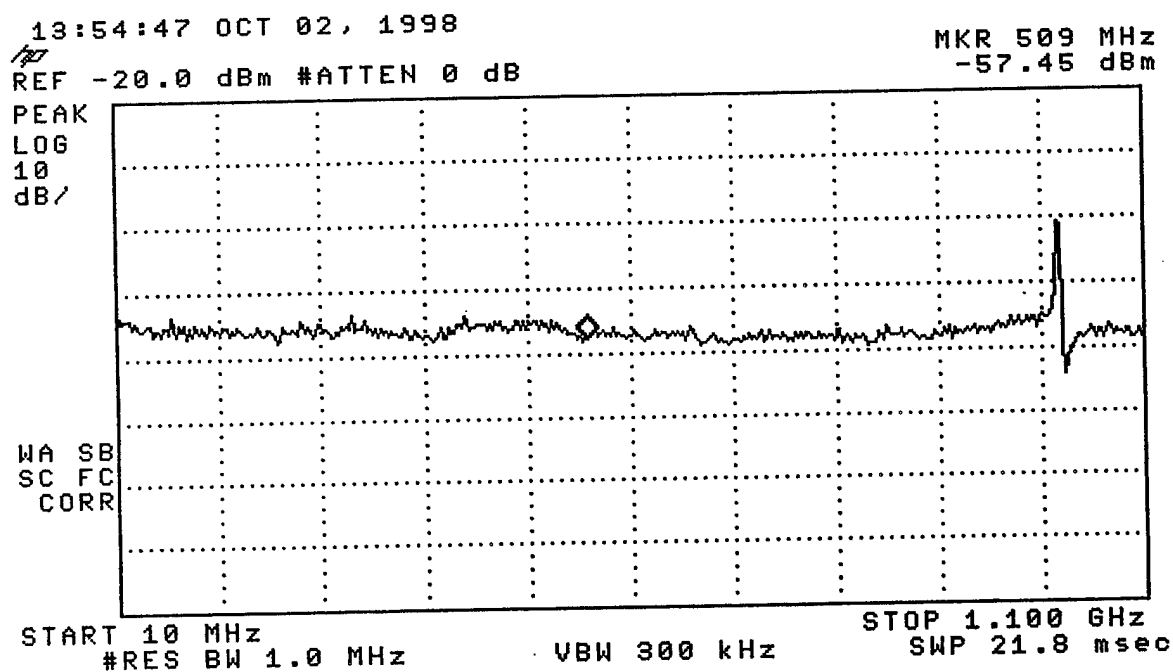
Figure 8. System noise floor

Figure 9. Swept frequency response of the sensor

18

High Frequency Test, 7GHz to 10 GHz

Figure 10 shows the schematic diagram of the system for testing the electric field sensor by placing it in a WR112 metallic waveguide fabricated by MITEC Eelctronics Ltd. The optical source is a low-noise Nd:YAG laser, Model 125 manufactured by Lightwave Electronics, Inc., operating at 1.3 micron wavelength. The optical receiver, Model 1411, is manufactured by New Focus, Inc. The output of the optical receiver is amplified by about 60dB using a low-noise amplifier.

The RF field used to modulate the sensor was produced using an RF oscillator and RF waveguide system. A computer running LabVIEW for Windows controlled the amount of current into the YIG (Yittrium Iron Garnet) oscillator. The YIG converts the current into an RF signal that is carried to the metallic waveguide.
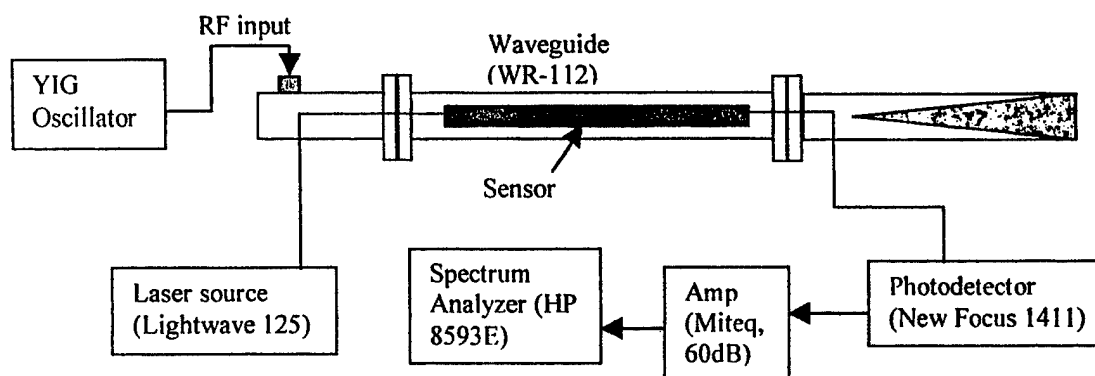
Figure 10. High frequency test set up

The waveguide WR112 covers the frequency range of 7 to 10GHz. The waveguide consists of an input section to launch the RF power, a straight sections in which the sensor is placed, and a conical load section to absorb the RF energy. A fiber optic feedthrough is incorporated at the input and the load sections to allow entry of the fiber cables into and out of the waveguide. The maximum electric field inside the waveguide is given by (Ref. 9)

$$E_{max} = \sqrt{\frac{P\,480\pi}{ab} \times \frac{1}{\sqrt{1 - \left(\frac{c}{f\,2a}\right)^2}}} \qquad (12)$$

where,

P = input power to the waveguide
a,b = width and height, 28.5 mm and 12.6 mm, respectively
c = velocity of light
f = microwave frequency

The RF input power to the waveguide of 7.37 dBm (5.5 mW) is supplied from a YIG oscillator. The electric field sensor was tested at a frequency of 8GHz. Using the above equation, the peak electric field inside the waveguide is calculated to be 175 Volts/meter.

Figures 11 and 12 show the system noise floor and the measured signal produced by the electric field sensor when the waveguide is excited at 8GHz. The noise floor and signal measured at 8GHz are -107 dBm/Hz and -31 dBm, respectively. Therefore, the internal electric field of 175 Volts/meter produces an SNR of 76 dB. The minimum detectable electric field is

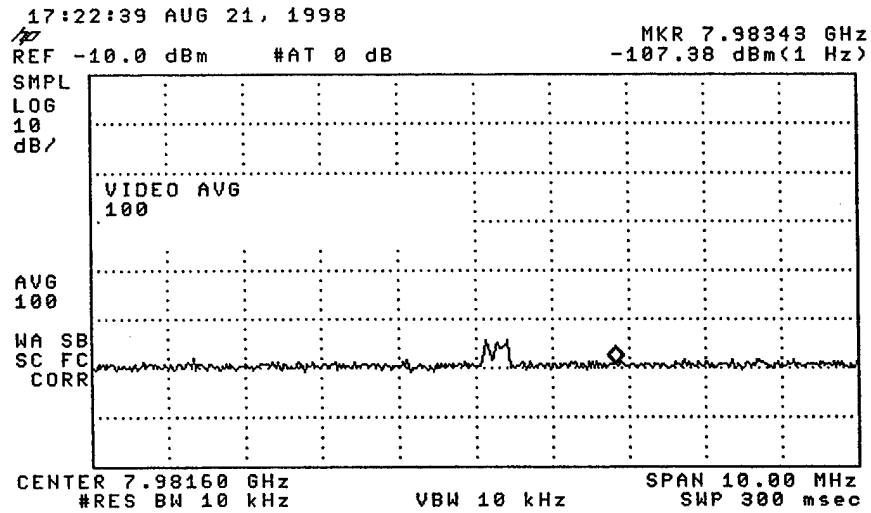$$E_{min} = 175 \times 10^{-\frac{76}{20}} = 28 \ (mV/m/\sqrt{Hz}) \qquad (13)$$

```
 17:22:39 AUG 21, 1998
/p̸⃗
REF -10.0 dBm      #AT 0 dB
```
```
                                      MKR 7.98343 GHz
                                      -107.38 dBm(1 Hz)
```


Figure 11. System noise floor

```
 17:18:44 AUG 21, 1998
/p̸⃗
REF -10.0 dBm      #AT 0 dB
```
```
                                      MKR 7.98368 GHz
                                      -31.34 dBm
```
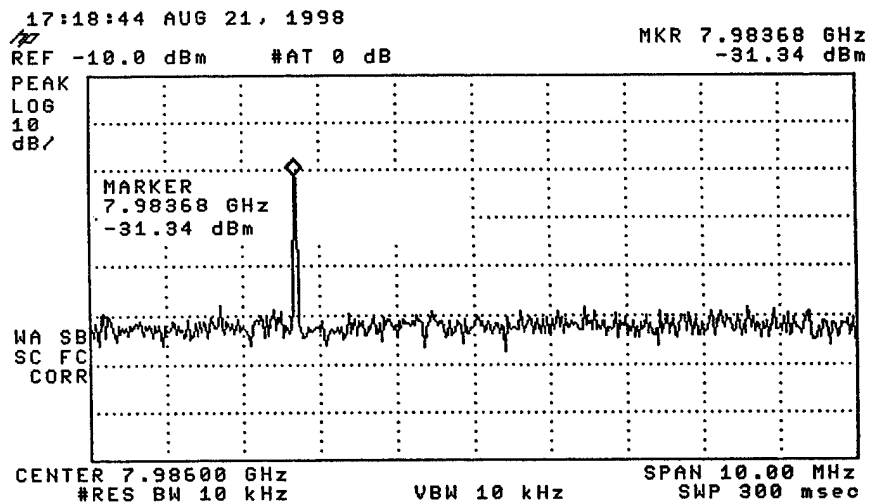

Figure 12. Sensor response at 8GHz

21

Use of Optical Filter to Increase Dynamic Range

Figure 13 shows the schematic diagram of the system for testing the electric field sensor by placing it in a WR75 metallic waveguide. This test uses the optical source and the receiver used in the high frequency test. As before, the RF input power to the waveguide is supplied from a YIG oscillator.

Figure 13 shows the experimental setup with the optical filter in the system. Using the dc voltage the filter was tuned to null the carrier frequency resulting in a null in the optical power. The amount of optical power that could be brought to the photodetector in this demonstration when the optical carrier was centered on a null, was about 10 μW.

Ideally, this feasibility demonstration should have been carried out with about 1 mW at the photodetector when the carrier frequency was in the null. However, attenuation of the E-field sensor used as the intensity modulator and the 3 to 4 dB excess loss of the PIRI filter itself, prevented the optical power from being sufficiently high. This did not invalidate the benefit of using the filter, only that the full relative 21 dB improvement in SNR is only available if, when the filter is tuned into a null, the mean optical power reaching the photodetector is close to the optical saturation power of that photodetector.

Figure 14 illustrates the results of the comparison tests using the MITEQ post-detection LNA system. The dc bias monitor voltage is used to tune the filter to null the optical carrier power at the receiver. The null in the optical carrier power corresponds to a dc voltage of approximately 3 mV. The receiver had a dc offset of 1 mV. The electric field sensor in the waveguide was modulated at 12.5 GHz and the modulated signal was observed and measured using the spectrum analyzer. The signal-to-noise ratio (SNR) with the filter in the system was measured to be 30.7 dB with respect to a 100 kHz bandwidth, and 9.2 dB without the filter. **Thus, the improvement in signal-to-noise ratio was 21.5 dB.**
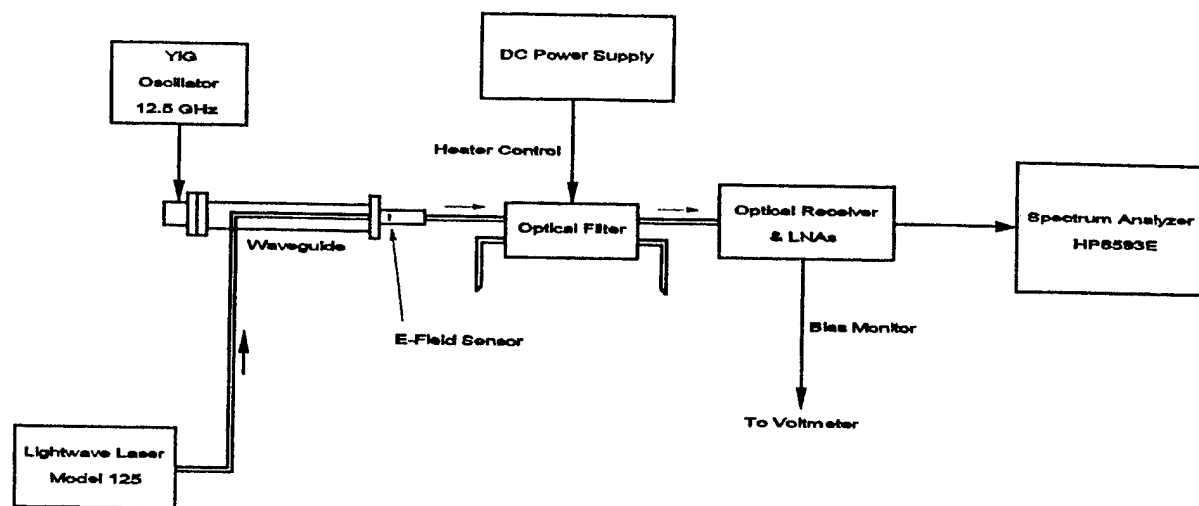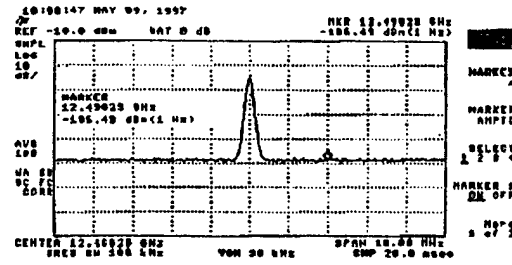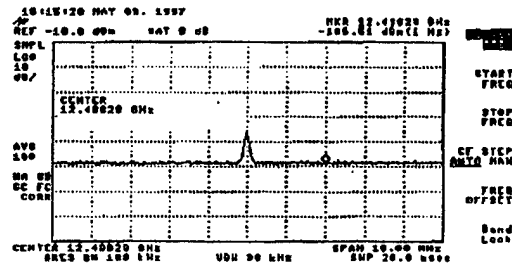
Figure 13. Carrier suppression test set up

Figure 14. Signal-to-noise ratio with and without optical carrier suppression filter

Signal-To-Noise Ratio with and without optical carrier suppression filter using the MITEQ post-detection LNA system.

Amplitude = 10 dB/div

Center Frequency = 12.5 GHz

Span = 10 MHz

Noise Equivalent Bandwidth = 120 kHz

Optical receiver DC output at null = 3 mV

Optical receiver DC offset = 1 mV

Received optical power at null = -25 dBm (3.2 μW)

(a)   With optical filter
Signal = -25.0 dBm
Noise = -106.5 dBm/Hz
SNR = 30.7 dB re 100 kHz

(b)   Without optical filter
Signal = -46.5 dBm
Noise = -106.5 dBm/Hz
SNR = 9.2 dB re 100 kHz

SNR Improvement = 21.5 dB

24

Conclusions

SRICO developed and delivered a wideband photonics electric field sensing system capable of measuring signals up to 18 GHz. The minimum detectable electric field was measured to be of 28 mV/m in a 1 Hz bandwidth; this surpassed the target specification of 100 mV/m in a 1Hz bandwidth. The technique of suppressing the optical carrier was shown to obtain a dynamic range greater than 40 dB.

This system could be successfully used inside an aircraft as an electromagnetic event sensing and recording system (EMESR) to monitor and record the electromagnetic (EM) event in various locations where the EM energy is suspected of causing electronic system upset and failure. The system would consist of passive wideband photonic electric field sensor probes located at critical locations in an aircraft, particularly the avionics bay, the main fuselage section, the tail assembly and the wings. The information would be transmitted via fiber optics cable to the signal processing and recording systems. The ability to monitor and record, in real time, electromagnetic events is of critical value to the operational Air Force. Such a device can reduce the down time of an aircraft experiencing reliability problems by providing the diagnostic technician with data collected during actual flight when all onboard systems are up and running. As a diagnostic tool, this sensor will help to significantly reduce costly, unnecessary maintenance requests by targeting the exact cause of electronic system failure. This approach completely eliminates the need to swap out suspected faulty modules until the aircraft system functions within specifications. More importantly, this data will directly contribute to the safety of the aircraft and its passengers as well as future aircraft that carry the same type of electronic equipment.

References

1. B. Clough, "A Review of Digital Flight Control System Upsets Caused by Electromagnetic Interference," USAF Wright Laboratory. Presented at AEROTECH '90, 3 October 1990.

2. S. Sriram, S.A. Kingsley and J.T. Boyd, "Electro-Optical Sensor for Detecting Electric Fields," U.S. Patent No. 5,267,336, 30 November 1993.

3. C.H. Bulmer, W.K. Burns and R.P. Moeller, "Linear Interferometric Waveguide Modulator for Electromagnetic Field Detection," Optics Letters 5, pp. 176-178 (1980).

4. Amnon Yariv, Quantum Electronics, John Wiley and Sons, New York (1975).

5. Properties of Lithium Niobate, EMIS Datareviews Series No. 5, Published by INSPEC, The Institution of Electrical Engineers, London and New York (1989).

6. W.K. Pratt, Laser Communication Systems, John Wiley and Sons, New York (1969).

7. M.J. LaGasse, W. Charczenko, M.C. Hamilton and S. Thaniyavran, "Optical Carrier Filtering for High Dynamic Range Fiber Optic Links," Electronics Letters , No. 25, pp. 2157-2158 (1994).

8. E.L. Wooten, R.L. Stone, E.W. Miles and E.M. Bradley, "Rapidly Tunable Narrowband Wavelength Filter using Lithium Niobate Unbalanced Mach-Zehnder Interferometers," J. Lightwave Technology, vol. 14, No. 11, pp. 2530-2536 (1996).

9. Handbook of Microwave Technology, Academic Press, San Diego (1995).

MISSION
OF
AFRL/INFORMATION DIRECTORATE (IF)

The advancement and application of information systems science and

technology for aerospace command and control and its transition to air,

space, and ground systems to meet customer needs in the areas of Global

Awareness, Dynamic Planning and Execution, and Global Information

Exchange is the focus of this AFRL organization. The directorate's areas

of investigation include a broad spectrum of information and fusion,

communication, collaborative environment and modeling and simulation,

defensive information warfare, and intelligent information systems

technologies.